Power Electronic Systems
Laboratory

IEEE Transactions on Industrial Electronics, Vol. 59, No. 9, pp. 3635-3647, September 2012.

A Three-Phase Delta Switch Rectifier for Use in Modern Aircraft

M. Hartmann
J. Miniböck
J. W. Kolar

Eidgenössische Technische Hochschule Zürich
Swiss Federal Institute of Technology Zurich

A Three-Phase Delta Switch Rectifier for Use in Modern Aircraft

Michael Hartmann, *Student Member, IEEE*, Johann Miniboeck, Hans Ertl, *Member, IEEE*, and Johann W. Kolar, *Fellow, IEEE*

***Abstract*—In the course of the More Electric Aircraft program frequently active three-phase rectifiers in the power range of several kilowatts are required. It is shown that the three-phase Δ-switch rectifier (comprising three Δ-connected bidirectional switches) is well suited for this application. The system is analyzed using space vector calculus and a novel PWM current controller modulation concept is presented, where all three phases are controlled simultaneously; the analysis shows that the proposed concept yields optimal switching sequences. Analytical relationships for calculating the power components average and rms current ratings are derived to facilitate the rectifier design. A laboratory prototype with an output power of 5 kW is built and measurements taken from this prototype confirm the operation of the proposed current controller. Finally, initial EMI-measurements of the system are also presented.**

***Index Terms*—Aerospace electronics, input current quality, pulse width modulation, three-phase rectifier.**

I. Introduction

In CONVENTIONAL civil aircraft, the flight control surfaces, such as the rudder, elevator, and aileron, are activated by hydraulic actuator systems. In course of the "More Electric Aircraft" (MEA) concept, these actuators will be replaced by Electro Hydrostatic Actuators (EHA) or Electro Mechanical Actuators (EMA) in order to reduce the weight of the aircraft which finally increases the total efficiency of the aircraft [1]–[3].

The MEA-concept in general calls for a reduction in the size and weight of the electrical systems. A major issue is the weight reduction of the power generation system by eliminating the generator gearbox used to obtain a three-phase 115 V_{rms} mains with a fixed frequency of 400 Hz. This results in a variable mains frequency of 360 Hz. . .800 Hz. Due to the increased power demands of modern aircraft, besides the variable mains frequency, the mains voltage will be increased to 230 V and the dc bus voltage will be increased from 270 V_{dc} to 540 V_{dc} [4]. In addition, the electronic systems must have very high reliability, i.e., the loss of one phase must not result in an outage of the rectifier system. Due to the unidirectional nature of power generation and the absence of a storing element in the aircraft, the loads are typically not allowed to feed back energy into the mains. Feedback of energy may be allowed in future aircraft and a study of the use of a local dc distribution system including an energy storage system element can be found in [5]. Due to the very rigorous current harmonic limits of present airborne system standards, converters with low THD of the input current and a high total power factor are required.

TABLE I
Typical Specifications of Active Three-Phase Rectifiers in Aircraft Applications

V_{Ni}	115 V ± 15%
f_{N}	360 Hz . . . 800 Hz
V_{o}	400 V_{DC}
P_{o}	5 kW . . . 10 kW

Direct ac–ac conversion using matrix converters or (non-regenerative) back-to-back voltage source or current source converters can be applied to implement such systems. In [6] the successful implementation of a matrix converter-based ac ground power supply is shown. According to the topology evaluation given in [7] the voltage source back-to-back solution may result in a lower weight which is of great importance in aircraft applications. The weight and size of the analyzed converter systems are strongly dependent on the voltage and power levels of the intended application and no general statement about size and weight can hence be given here. In this paper, a three-phase rectifier system for the specifications given in Table I, which may also be used as the front end of the voltage source back-to-back solution, will be discussed.

In [8], it has been shown that the 6-switch three-level Vienna-type rectifier topology [cf. Fig. 1(a)] [9] is very well suited to aircraft applications. This topology's main feature is a reduced semiconductor voltage stress, something especially important for high-output voltage levels, and is a good solution for the increased mains voltage of 230 V_{rms} in future aircraft. However, the tradeoff is increased conduction losses since there are always two semiconductors connected in series per phase. Two-level three-phase rectifier topologies may show greater efficiency but suffer from higher semiconductor voltage stress.

High-efficiency switches (CoolMOS) with a blocking voltage of 600 V and an on-state resistance $R_{\mathrm{DSon}} < 100$ mΩ are commercially available for the desired output voltage level of

Manuscript received September 9, 2010; revised March 30, 2011; accepted May 16, 2011. Date of publication June 7, 2011; date of current version April 13, 2012.

M. Hartmann and J. W. Kolar are with the Power Electronic Systems Laboratory, ETH Zurich, 8092 Zurich, Switzerland (e-mail: hartmann@lem.ee.ethz.ch; kolar@lem.ee.ethz.ch).

J. Miniboeck was with the Power Electronic Systems Laboratory, ETH Zurich, 8092 Zurich, Switzerland, and now with M-PEC Power Consulting, 3752 Walkenstein, Austria (e-mail: miniboeck@mpec.at).

H. Ertl is with the Power Electronics Section, Vienna University of Technology, 1040 Vienna, Austria (e-mail: j.ertl@tuwien.ac.at).

Color versions of one or more of the figures in this paper are available online at http://ieeexplore.ieee.org.

Digital Object Identifier 10.1109/TIE.2011.2158770

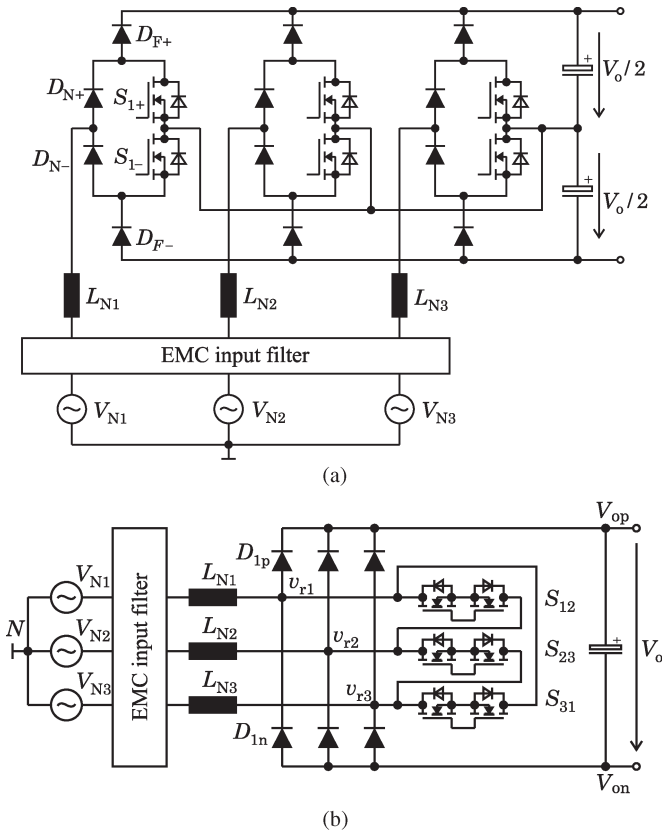

Fig. 1. Active three-phase rectifiers suitable for aircraft applications; (a) three-level 6-switch Vienna-type rectifier and (b) two-level Δ-switch rectifier.

$V_o = 400\ V_{dc}$. A reduction of the voltage stress, as given by three-level topologies such as the Vienna-Rectifier concept, is therefore not needed. Several two-level three-phase rectifier topologies are presented in the literature and a comparative study can be found in [11], [12]. The application of a standard six-switch PWM-rectifier bridge is unsuitable due to its bidirectional power flow behavior. Additional drawbacks are reduced reliability due to possible shoot-through of a bridge leg, resulting in a short circuit of the dc-voltage, the high current levels of the semiconductors and the involvement of the MOSFET body diode, causing a substantial limitation of the switching frequency.

In order to improve input current quality, the concept of third harmonic injection can be applied. The Minnesota rectifier [14], [15] implements a current injection into all three phases using a zigzag connected transformer in combination with boost-type output stages which yields to a controlled output voltage. The required low-frequency magnetic parts inhibit, however, the application of this promising approach in aircraft applications. Topologies with a current injection only into one phase have therefore been developed [16], [17] but these topologies are not further discussed here as they are not able to handle a single phase loss.

In [18], a topology using either Y-connected or Δ-connected [cf. Fig. 1(b)] bidirectional switches on the ac-side is presented and the operation analysis of the Δ-version using space vector modulation in combination with hysteresis control is discussed in [19]. In general, the Y-connected implementation shows higher conduction losses as compared to the Δ-connected alternative, as there are always two (bidirectional) switches connected in series. A short circuit of the dc-voltage is not possible with either topology. Fig. 2 shows two possibilities of implementing the bidirectional (current), bipolar (voltage) switches. The original Vienna-Rectifier topology uses the bidirectional switch shown in Fig. 2(b) instead of the two MOSFETs per phase-leg shown in Fig. 1(a). An elegant topology, which integrates the bidirectional switch of Fig. 2(b) into the diode bridge, is shown in [20], [21]. The conduction losses of this version are higher than those when two MOSFETs [Fig. 1(a)] are used. In addition, some topologies using quasi tri-directional switches [22] or topologies operating in discontinuous conduction mode are shown [23], [24]. The topology using tri-directional switches increases the system complexity and discontinuous-mode topologies are unable to fulfill the requirements on the total harmonic distortion. Due to its low complexity, low conduction losses, and high reliability, the Δ-switch rectifier topology seems to be an optimal choice for implementation of a rectifier for aerospace applications with the requirements given in Table I.

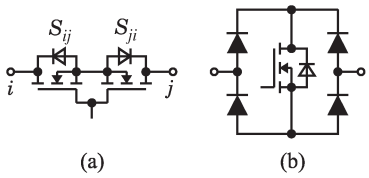

Fig. 2. Possible implementations of a bidirectional (current), bipolar (voltage) switch using (a) two MOSFETs and (b) MOSFET and a diode bridge.

In addition to efficiency and power density, control issues also influence the practical applicability of the circuit topology. Several possibilities for the control of three-phase rectifiers exist and a survey of these methods can be found in [25]. A control method based on low switching frequencies is given in [26] but this method cannot be used for the desired application because of the high ac current harmonics. A hysteresis controller, as shown in [27], would be an easy way to control the rectifier system, but its varying switching frequency may increase the effort of EMI filtering. A controller using the one-cycle control method is shown in [28], but there the controller structure has to be changed over every 60° and the input current control is always limited to 2 phases. A concept for mains proportional input current shaping without the need of multipliers, which is advantageous for an analog implementation, can be found in [10]. In [29], a PWM-control method for the rectifier system is proposed but no information is given about the exact switching sequence of the switches, which mainly influences the efficiency of the rectifier system. In this paper, the PWM-control method shown in [30] which is based on triangular carrier signals is discussed in more detail. Using this control method, all three phases are controlled simultaneously. The resulting optimal switching sequences, differential mode (DM), and common mode (CM) noise sources are analyzed by application of space vector calculus. In addition, the proposed control method is able to handle a phase loss without changing the controller structure which is verified by experimental results.

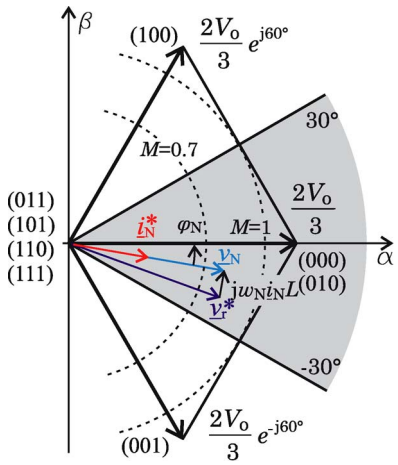

Fig. 3. Space vector diagram of the Δ-switch rectifier for the sector $\varphi_N \in [-30°, +30°]$.

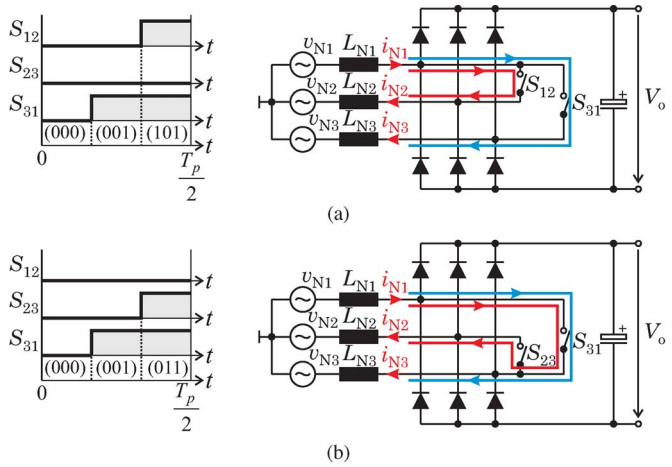

Fig. 4. Possible switching sequences for $\varphi_N = -15°$ and equivalent circuits for the time interval where both switches are on. (a) Sequence A: (000)-(001)-(101)-(001)-(000), S_{23} = OFF. (b) Sequence B: (000)-(001)-(011)-(001)-(000), S_{12} = OFF.

II. System Operation

The three switches $S_{ij}(i, j \in \{1, 2, 3\})$ of Fig. 1(b) are used to generate sinusoidal input currents which are proportional to the mains voltage. The discrete converter voltage space vector can be calculated by

$$\underline{v}_r = \frac{2}{3}(v_{r1} + \underline{a}v_{r2} + \underline{a}^2 v_{r3}) \text{ with } \underline{a} = e^{j\frac{2\pi}{3}}. \quad (1)$$

The possible converter voltages v_{ri} are dependent on the state of the switches s_{ij} ($s_{ij} = 1$ denotes the turn-on state of switch S_{ij}) and on the direction of the input phase currents i_{Ni}. Therefore, the available voltage space vectors change over every 60° interval of the mains period. If (s_{12}, s_{23}, s_{31}) describes the different switching states, the resulting voltage space vectors for $\varphi_N \in [-30°, 30°]$ $(i_{N1} > 0, i_{N2} < 0, i_{N3} < 0)$ can be calculated as

$$(000), (010) : \underline{v}_{r_1} = \frac{2}{3}V_o \quad (2)$$

$$(001) : \underline{v}_{r_2} = \frac{2}{3}V_o e^{-j60°} \quad (3)$$

$$(100) : \underline{v}_{r_3} = \frac{2}{3}V_o e^{j60°} \quad (4)$$

$$(011), (101), (110), (111) : \underline{v}_{r_4} = 0 \quad (5)$$

(cf. Fig. 3).

Only states (000), (001), (010), and (100) show a non-zero magnitude and the voltage space vector of (010) is equal to the space vector for state (000). In each 60°-sector, there is a redundancy of the (000)-vector and therefore only 4 different voltage space vectors can be generated by the converter in each sector. These discrete voltage space vectors are used to approximate the converter's voltage reference vector

$$\underline{v}_r^* = \underline{\hat{V}}_r^* e^{j\varphi_{\underline{v}_r}}, \qquad \varphi_{\underline{v}_r} = \omega_N t \quad (6)$$

in the time average over the pulse period. In conjunction with the mains voltage system

$$\underline{v}_N = \underline{\hat{V}}_N e^{j\varphi_{\underline{v}_N}} \quad (7)$$

the voltage difference

$$\underline{v}_N - \underline{v}_r^* = L\frac{d\underline{i}_N^*}{dt} \quad (8)$$

leads to the input current

$$\underline{i}_N^* = \underline{\hat{I}}_N^* e^{j\varphi_{\underline{i}_N^*}} \quad (9)$$

if only average values over one pulse period are considered. All voltage space vectors with two or three switches in the on-state are redundant and hence only two switches can be used to control the input currents. The remaining switch can therefore be permanently off in this sector. Two different reasonable switching sequences with minimum number of switching actions, where always only the switching action of one switch yields to the next switching state, can be generated in each 60°-sector. Fig. 4 shows the corresponding modulation signals of the bidirectional switches ($\varphi_N = -15°$), and equivalent circuits are given for the time interval where both switches are on. For sequence A [(000)-(001)-(101)-(001)-(000), S_{23} = OFF], the positive input current i_{N1} is shared by S_{12} and S_{31} dependent on the on-states of the switches. In contrast to sequence A, the whole current i_{N1} is carried by switch S_{31} for sequence B [(000)-(001)-(011)-(001)-(000), S_{12} = OFF] during the state (011). This results in higher conduction losses and therefore sequence A is preferable.

The corresponding pulsating rectifier phase voltages

$$v_{ri} = v_{DMi} + v_{CM} \quad (10)$$

can be separated into a differential voltage part v_{DMi} which controls the input current and a common mode voltage part v_{CM}. The CM voltage is equal to all three phases and is given by

$$v_{CM} = \frac{V_{op,N} + V_{on,N}}{2} \quad (11)$$

where the bus voltages $V_{op,N}$ and $V_{on,N}$ are measured with respect to ground N [cf., Fig. 1(b)].

TABLE II
CALCULATED VOLTAGE SPACE VECTORS $\underline{v}_{\mathrm{r}}$, PHASE VOLTAGES INCLUDING CM PARTS $v_{\mathrm{r}i}$ PHASE VOLTAGES WITHOUT CM PARTS $v_{\mathrm{DM}i}$ AND CM VOLTAGE v_{CM} IN DEPENDENCY OF THE SWITCHING STATE (s_{12}, s_{23}, s_{31}) FOR $\varphi_{\mathrm{N}} \in [-30°, +30°]$

	$v_{\mathrm{r}1}$	$v_{\mathrm{r}2}$	$v_{\mathrm{r}3}$	$v_{\mathrm{DM}1}$	$v_{\mathrm{DM}2}$	$v_{\mathrm{DM}3}$	v_{CM}	$\underline{v}_{\mathrm{r}}$
(0 0 0)	$\frac{1}{2}V_{\mathrm{o}}$	$-\frac{1}{2}V_{\mathrm{o}}$	$-\frac{1}{2}V_{\mathrm{o}}$	$\frac{2}{3}V_{\mathrm{o}}$	$-\frac{1}{3}V_{\mathrm{o}}$	$-\frac{1}{3}V_{\mathrm{o}}$	$-\frac{1}{6}V_{\mathrm{o}}$	$\frac{2}{3}V_{\mathrm{o}}$
(0 0 1)	$\frac{1}{2}V_{\mathrm{o}}$	$-\frac{1}{2}V_{\mathrm{o}}$	$\frac{1}{2}V_{\mathrm{o}}$	$\frac{1}{3}V_{\mathrm{o}}$	$-\frac{2}{3}V_{\mathrm{o}}$	$\frac{1}{3}V_{\mathrm{o}}$	$\frac{1}{6}V_{\mathrm{o}}$	$\frac{2}{3}V_{\mathrm{o}}e^{-j60°}$
(0 1 0)	$\frac{1}{2}V_{\mathrm{o}}$	$-\frac{1}{2}V_{\mathrm{o}}$	$-\frac{1}{2}V_{\mathrm{o}}$	$\frac{2}{3}V_{\mathrm{o}}$	$-\frac{1}{3}V_{\mathrm{o}}$	$-\frac{1}{3}V_{\mathrm{o}}$	$-\frac{1}{6}V_{\mathrm{o}}$	$\frac{2}{3}V_{\mathrm{o}}$
(1 0 0)	$\frac{1}{2}V_{\mathrm{o}}$	$\frac{1}{2}V_{\mathrm{o}}$	$-\frac{1}{2}V_{\mathrm{o}}$	$\frac{1}{3}V_{\mathrm{o}}$	$\frac{1}{3}V_{\mathrm{o}}$	$-\frac{2}{3}V_{\mathrm{o}}$	$\frac{1}{6}V_{\mathrm{o}}$	$\frac{2}{3}V_{\mathrm{o}}e^{j60°}$
(0 1 1)	0	0	0	*)	*)	*)	*)	0
(1 0 1)	0	0	0	*)	*)	*)	*)	0
(1 1 x)	0	0	0	*)	*)	*)	*)	0

*) CM voltage is not defined by the switching state – only by parasitic elements.

Table II summarizes the voltage space vectors $\underline{v}_{\mathrm{r}}$, phase voltages including CM parts $v_{\mathrm{r}i}$, phase voltages without CM parts $v_{\mathrm{DM}i}$ and corresponding CM part v_{CM} in dependency of the switching state (s_{12}, s_{23}, s_{31}) for $\varphi_{\mathrm{N}} \in [-30°, +30°]$. Should two or three switches be closed, all three input phases are shorted, no bridge diode is conducting and therefore no connection between the dc-side and the ac-side exists. The CM voltage is therefore not defined by the switching states during this time period. A CM voltage will appear in practice which depends on parasitic circuit elements e.g., reverse blocking currents of the rectifier diodes $D_{i\mathrm{p}}$ and $D_{i\mathrm{n}}$, parasitic capacitances of the semiconductors to the heat sink, etc. The required attenuation of the CM filter stage therefore has to be carefully analyzed at the practically implemented prototype. It also has to be noted here that the Δ-switch rectifier topology is not able to actively generate a CM voltage e.g., for third harmonic injection.

If equal reverse blocking currents of the rectifier bridge diodes are assumed and if parasitic capacitances to the heat sink or to earth are neglected, the DM and CM voltage waveforms given in Fig. 5 can be determined. The DM voltage shows voltage steps with a magnitude of $(2/3)V_{\mathrm{o}}$ whereas the CM voltage, as already analyzed in [36], shows only an amplitude of $(1/6)V_{\mathrm{o}}$ in the case of an ideal symmetrical system. It is also obvious that the applied modulation scheme (cf., Section III) yields to a low-frequency CM part. The CM voltage waveform, however, changes completely if parasitic capacitances are considered. At least for the design of the DM filter stage, the voltage waveform shown in Fig. 5 can be used, for instance to apply the filter design procedure presented in [31].

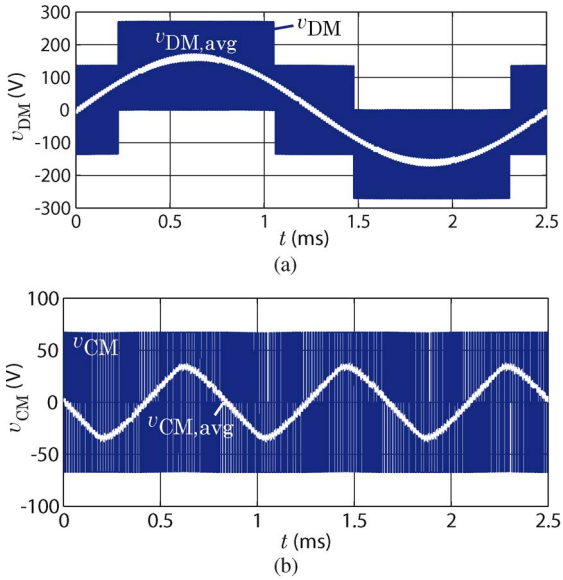

Fig. 5. Simulated voltage waveforms of the rectifier system operated at $P_{\mathrm{o}} = 5$ kW and $f_{\mathrm{N}} = 400$ Hz; (a) DM voltage and (b) predicted CM voltage if a symmetrical diode bridge, e.g., equal reverse blocking currents, is assumed.

III. PWM CURRENT CONTROLLER

The aim of the current controller is to force the input currents of each phase to follow the (sinusoidal) mains voltages. The Δ-connected switches directly influence the line-to-line voltages. The idea of controlling these Δ-related currents arises. This is unfortunately not very convenient due to the necessary clamping actions caused by the large number of redundant switching states. This can be avoided if the phase currents $i_{\mathrm{N}i}$ of the rectifier are controlled. The resulting phase modulation signals then have to be transferred to Δ-oriented quantities. In this way all three currents can be permanently controlled and the necessary clamping actions are performed in a final logical unit just before the PWM-signals s_{ij} are transferred to the switches.

The structure of the proposed current controller is shown in Fig. 6. All three input currents $i_{\mathrm{N}i}$ are sensed by appropriate current sensors and compared with the reference current $i^*_{\mathrm{N}i}$. The reference current is generated by multiplying the mains voltage $v_{\mathrm{N}i}$ by a reference conductance g^*_{e} (defined by the superimposed output voltage controller $F(s)$) in order to achieve ohmic input current behavior. The current controller $K_{\mathrm{I}}(s)$ (implemented as P-type controller), together with a mains voltage feedforward signal [32], generates the required converter phase voltages $v^*_{\mathrm{r}\mathrm{N}i}$. The bidirectional switches are connected between two phases and therefore the corresponding equivalent line-to-line converter voltages

$$v^*_{\mathrm{r}12} = v^*_{\mathrm{r}\mathrm{N}1} - v^*_{\mathrm{r}\mathrm{N}2} \tag{12}$$

$$v^*_{\mathrm{r}23} = v^*_{\mathrm{r}\mathrm{N}2} - v^*_{\mathrm{r}\mathrm{N}3} \tag{13}$$

$$v^*_{\mathrm{r}31} = v^*_{\mathrm{r}\mathrm{N}3} - v^*_{\mathrm{r}\mathrm{N}1} \tag{14}$$

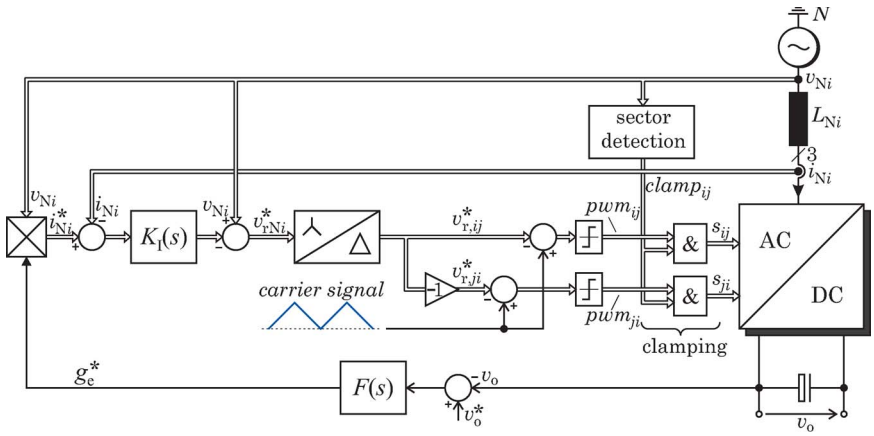

Fig. 6. Structure of the proposed PWM current controller. Signal paths being equal for different phases are shown by double lines.

TABLE III
REQUIRED CLAMPING ACTIONS; 0 INDICATES THAT THE CORRESPONDING MOSFET IS PERMANENTLY OFF; 1 PERMANENTLY ON AND pwm_{ij} THAT THE MOSFET IS MODULATED BY THE CURRENT CONTROLLER

	s_{12}	s_{21}	s_{23}	s_{32}	s_{13}	s_{31}
$330° \ldots 30°$	pwm_{12}	1	0	0	pwm_{13}	1
$30° \ldots 90°$	0	0	pwm_{23}	1	pwm_{13}	1
$90° \ldots 150°$	1	pwm_{21}	pwm_{23}	1	0	0
$150° \ldots 210°$	1	pwm_{21}	0	0	1	pwm_{31}
$210° \ldots 270°$	0	0	1	pwm_{32}	1	pwm_{31}
$270° \ldots 330°$	pwm_{12}	1	1	pwm_{32}	0	0

are needed for PWM-generation. The star-delta transformation is followed by two PWM-modulators which generate the PWM-signals for the MOSFETs of the bidirectional switches [bidirectional switches are implemented according to Fig. 2(a)]. In general, dependent on the current direction of the bidirectional switch, only one MOSFET has to be gated. If the second MOSFET is permanently off during this time, the current is carried by its body diode. The body diode shows a relative large forward voltage which yields to higher conduction losses. These losses can be reduced by the low-impedance path of the MOSFET channel, if the second MOSFET is turned on as well. As the current direction of the switch only changes every 120°, this MOSFET can be permanently on during this time interval. Two independent PWM-signals are therefore required for the bidirectional switches. As shown in Fig. 2(a), MOSFET S_{ij} connects port i of the bidirectional switch to port j and its PWM-signals are given by pwm_{ij}, respectively. The operation of the modulator will be discussed in the next section.

The clamping actions are controlled by a sector-detection unit which derives the clamping signals $clamp_{ij}$ from the mains voltage. The resulting clamping actions considering all 60°-sectors are summarized in Table III for all MOSFETs, whereas e.g., 0 indicates that the corresponding MOSFET is permanently off in this sector.

A. PWM-Modulator

A single unipolar triangle carrier signal is used (cf., Fig. 7) to implement the PWM-modulator. The modulator has to assure

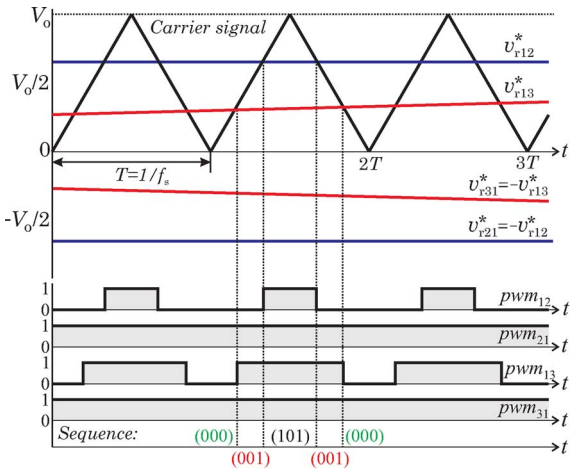

Fig. 7. PWM-modulation and resulting switching sequence at $\varphi_N = -15°$. Switches S_{23} and S_{32} are not shown, because they are permanently off in this sector. The resulting (optimal) sequence is (000)-(001)-(101)-(001)-(000).

an optimal switching sequence and has to generate the duty cycles

$$v^*_{rij} > 0 : \delta_{ij} = 1 - \frac{v^*_{rij}}{V_o}, \qquad \delta_{ji} = 1 \tag{15}$$

$$v^*_{rij} < 0 : \delta_{ij} = 1, \qquad \delta_{ji} = 1 - \frac{v^*_{rji}}{V_o}. \tag{16}$$

If the carrier signal is larger than the modulation voltage v^*_{rij}, the output of the modulator is high. Unlike the triangular signal, the modulation voltages v^*_{rij} are bipolar and hence a duty cycle of 100% is generated for negative modulation voltages. According to

$$v^*_{rij} = (-1) \cdot v^*_{rji} \tag{17}$$

one MOSFET of the bidirectional switch is always permanently on (i.e., S_{21} for $\varphi_N \in [-30°, 30°]$), which reduces the on-state losses of the device.

Fig. 7 shows the operation of the PWM-modulator at $\varphi_N = -15°$. The two modulation voltages v^*_{r21} and v^*_{r31} are negative and result in a duty cycle of 100%. According to Table III, switches S_{23} and S_{32} are permanently off in this sector and are

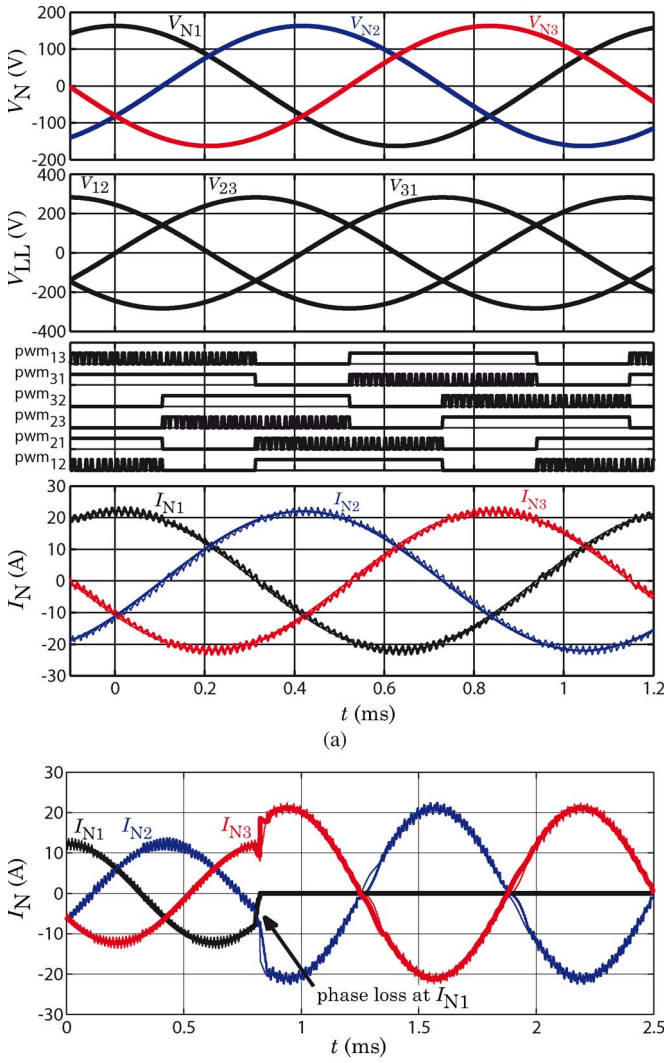

Fig. 8. Simulation results of the Δ-switch rectifier; (a) $V_{Ni} = 115\ V_{rms}$, $f_N = 800$ Hz, $V_o = 400\ V_{dc}$, $P_o = 5$ kW, $L_{Ni} = 330\ \mu$H and (b) phase loss of I_{N1} at $t = 0.85$ ms ($P_o = 3$ kW).

therefore not shown. The remaining voltages v^*_{r12} and v^*_{13} are used for modulation and result in the desired optimal switching sequence (000)-(001)-(101)-(001)-(000) (see also Fig. 4).

IV. Simulation Results

A digital computer simulation is used to confirm the operation of the proposed control technique. Fig. 8(a) demonstrates good performance of the proposed current controller at an input frequency of $f_N = 800$ Hz ($V_{Ni} = 115\ V_{rms}$, $V_o = 400\ V_{dc}$, $P_o = 5$ kW, $L_{Ni} = 330\ \mu$H). A switching frequency of 72 kHz is used and according to Fig. 8(a) the input currents i_{Ni} follow the sinusoidal 800-Hz input voltages V_{Ni}. The current ripple of the clamped phase is furthermore not higher than in the two controlled phases. It should be repeated that the current controller works permanently i.e., without any structural changes, and that only a logic-block just before the modulator output provides the necessary clamping actions. In Fig. 8(b) the system response on a phase loss at $t = 0.85$ ms is depicted. After some minor ringing, the system operates in 2-phase mode and it should be noticed that no changes in the controller structure or parameters are required to handle this fault condition.

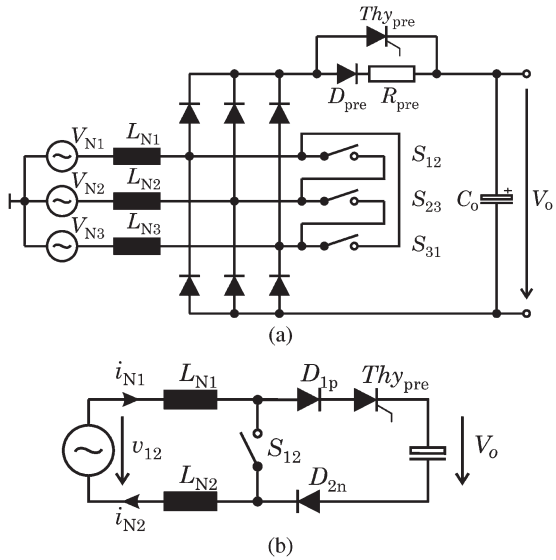

Fig. 9. (a) Proposed precharge circuit for start-up of the rectifier, consisting of precharge diode D_{pre}, precharge resistor R_{pre} and thyristor Thy_{pre} and (b) Equivalent circuit for switch S_{12} at $\varphi_N = -15°$.

V. System Design

In this section, some issues of the design and the practical implementation of the Δ-switch rectifier will be discussed.

A. Startup

A precharge circuit consisting of diode D_{pre}, resistor R_{pre}, and thyristor Thy_{pre} is applied on the dc-side of the rectifier [cf. Fig. 9(a)] in order to limit the in-rush current at start-up of the rectifier system. During start-up, the thyristor is off and the precharge resistor limits the inrush current. The thyristor is turned on as soon as the capacitors are completely charged to the peak value of the line-to-line voltage. The bidirectional switches are permanently off during startup (current controller is disabled during this time). According to Fig. 9(b), the thyristor is located within the commutation path of the rectifier (e.g., S_{12}, D_{1p}, Thy_{pre} and D_{n2}). In order to minimize the thyristors influence on the parasitic inductance of the commutation path, three thyristors (one thyristor closely placed to each switch) are used in parallel. This also reduces the on-resistance of the additional element advantageously.

B. Component Stresses

In order to determine the on-state losses of the semiconductors, the current rms and average values have to be calculated and simple analytical approximations are derived. It is assumed that the rectifier has

- a purely sinusoidal phase current shape;
- ohmic fundamental mains behavior;
- no low-frequency voltage drop across the boost inductor for the sinusoidal shaping of the input currents;

- a constant switching frequency;
- linear behavior of the boost inductors (inductance is not dependent on the current level);

for the following calculations.

1) Bidirectional Switches S_{ij}: Each bidirectional switch of Fig. 2(a) consists of two MOSFETs and hence two elements have to be considered: the MOSFET which is modulated by the current controller and the body diode of the second MOSFET. The current average values of the semiconductors are therefore not zero, although the entire average current of the bidirectional switch is zero (averaging within a full line-frequency fundamental period). With the defined modulation index

$$M = \frac{\sqrt{3}\widehat{V}_{\mathrm{N}}}{V_{\mathrm{o}}} \tag{18}$$

the average and rms currents of the two semiconductors forming the bidirectional switch finally result in

$$I_{\mathrm{T,avg}} = \widehat{I}_{\mathrm{N}} \left(\frac{1}{2\pi} - \frac{M}{4\sqrt{3}} \right) \tag{19}$$

$$I_{\mathrm{T,rms}} = \widehat{I}_{\mathrm{N}} \sqrt{\left(\frac{1}{6} - \frac{\sqrt{3}}{8\pi} \right) - \frac{M}{2\sqrt{3}\pi}}. \tag{20}$$

2) Diodes $D_{\mathrm{p}i}, D_{\mathrm{n}i}$: The average and rms currents of the rectifier diodes are

$$I_{\mathrm{D,avg}} = \widehat{I}_{\mathrm{N}} \frac{M}{2\sqrt{3}} \tag{21}$$

$$I_{\mathrm{D,rms}} = \widehat{I}_{\mathrm{N}} \sqrt{\frac{M(5+2\sqrt{3})}{12\pi}}. \tag{22}$$

3) Startup Thyristor Thy_i: The thyristor current is a combination of the diode currents, and results to

$$I_{\mathrm{Thy,avg}} = 3 \cdot I_{\mathrm{D,avg}} = \widehat{I}_{\mathrm{N}} \frac{M\sqrt{3}}{2} \tag{23}$$

$$I_{\mathrm{Thy,rms}} = \widehat{I}_{\mathrm{N}} \sqrt{\frac{5M}{2\pi}}. \tag{24}$$

4) Capacitor C_{o}: The rms current stress of the output capacitor for a constant load current I_{o} can be calculated using

$$I_{\mathrm{C,rms}} = \sqrt{I_{\mathrm{Thy,rms}}^2 - I_{\mathrm{Thy,avg}}^2} \tag{25}$$

which leads to

$$I_{\mathrm{C,rms}} = \widehat{I}_{\mathrm{N}} \sqrt{\frac{5M}{2\pi} - \frac{3M^2}{4}}. \tag{26}$$

5) Boost Inductor L_{boost}: In order to be able to design the boost inductors, the maximum amplitude of the input ripple current is needed. The maximum magnitude of the ripple current occurs at the point where the two operating switches show equal duty cycles e.g., $\varphi_{\mathrm{N}} = 0$ for phase L_1, as can also be verified using Fig. 8(a). A short calculation yields to

$$\Delta i_{\mathrm{L,pp,max}} = \frac{V_{\mathrm{o}}}{\frac{3}{2} L_{\mathrm{N}} f_{\mathrm{s}}} \frac{\sqrt{3}}{2} M \left(1 - \frac{\sqrt{3}}{2} M \right). \tag{27}$$

The required boost inductor in order to limit the ripple current to $\Delta i_{\mathrm{L,pp,max}} = k\widehat{I}_{\mathrm{N}}$ is therefore given by

$$L_{\mathrm{N}} = \frac{V_{\mathrm{o}}}{k\widehat{I}_{\mathrm{N}} f_{\mathrm{s}}} \frac{M}{\sqrt{3}} \left(1 - \frac{\sqrt{3}}{2} M \right). \tag{28}$$

TABLE IV
ANALYTICALLY CALCULATED AND SIMULATED MEAN AND rms CURRENT VALUES OF THE SEMICONDUCTORS FOR $P_{\mathrm{o}} = 4$ kW, $V_{\mathrm{N}i} = 115\ V_{\mathrm{rms}} (M = 0.7)$, $f_{\mathrm{s}} = 72$ kHz, $L_{\mathrm{N}i} = 330\ \mu$H

	Simulated	**Calculated**
$\widehat{I}_{\mathrm{N}}$	16.5 A	16.5 A
$I_{\mathrm{T,avg}}$	0.98 A	0.95 A
$I_{\mathrm{T,rms}}$	3.09 A	3.0 A
$I_{\mathrm{D,avg}}$	3.33 A	3.35 A
$I_{\mathrm{D,rms}}$	6.53 A	6.56 A
$I_{\mathrm{Thy,avg}}$	10.0 A	10.06 A
$I_{\mathrm{Thy,rms}}$	12.3 A	12.35 A
$I_{\mathrm{C,rms}}$	7.16 A	7.16 A
$\Delta i_{\mathrm{L,pp,max}}$	2.6 A	2.67 A

TABLE V
SPECIFICATIONS OF THE LABORATORY PROTOTYPE IMPLEMENTED

Input voltage:	$v_{\mathrm{N}} = 97\,\mathrm{V_{rms}} \ldots 132\,\mathrm{V_{rms}}$
Input frequency:	$f_{\mathrm{N}} = 360\,\mathrm{Hz} \ldots 800\,\mathrm{Hz}$
Switching frequency:	$f_{\mathrm{s}} = 72\,\mathrm{kHz}$
Output voltage:	$v_{\mathrm{o}} = 400\,\mathrm{V_{DC}}$
Output power:	$P_{\mathrm{o}} = 5\,\mathrm{kW}$

The mean and rms currents for an output power of 4 kW and mains voltage of $V_{\mathrm{N}i} = 115\ V_{\mathrm{rms}}$ $(M = 0.7)$ have been calculated to verify the derived formulas. In Table IV the results of this calculation are compared to the results of a simulation and show good accuracy.

VI. LABORATORY PROTOTYPE

Based on the proposed controller concept, a laboratory setup of the Δ-switch rectifier according to the specifications given in Table V was built. The prototype is shown in Fig. 10. An existing EMI-filter, originally designed for a 72-kHz Vienna-type rectifier, was applied to this rectifier. The overall dimensions of the system are 170 mm $\times$ 120 mm $\times$ 128 mm, thus giving a power density of 1.91 kW/dm^3 (or 31.4 W/in^3). The system is forced air-cooled and has a weight of 3.78 kg resulting in a power to weight ratio of 1.32 kW/kg. The proposed controller is digitally implemented in a fixed-point Texas Instruments DSP (TI 320F2808) and a switching frequency of 72 kHz is used. The CoolMOS IPP60R045CP with a very low R_{DSon} of 45 mΩ is used to implement the bidirectional switches, and Si-diodes APT30D60BHB for the rectifier diodes. A summary of the employed devices is given in Table VI.

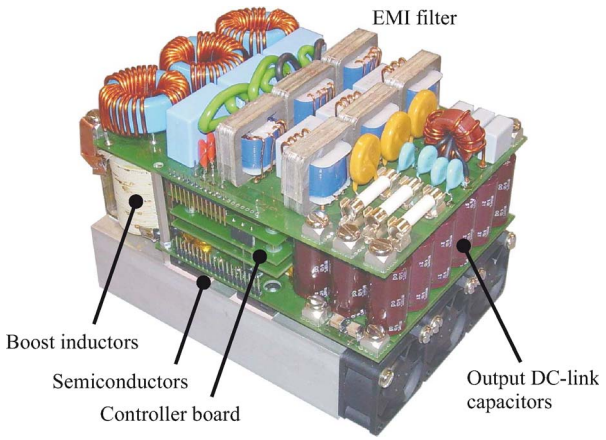

Fig. 10. 5 kW Δ-switch rectifier laboratory prototype. Dimensions: 170 mm × 120 mm × 128 mm (6.69 in × 4.72 in × 5.04 in).

TABLE VI
POWER DEVICES SELECTED FOR IMPLEMENTATION OF THE Δ-SWITCH RECTIFIER

Part	Device Description
S_{ij}	IPW60R045CP (CoolMOS)
D_{ni}, D_{pi}	APT30D60BHB (Ultrafast)
Thy_i	40TPS12A
C_o	18 x Nippon Chemicon KXG 82 μF/450 V in parallel
L_{Ni}	Schott HWT-193, 326 μH

A P-type current controller with a gain of $k_p = 0.25$ is used in combination with an input voltage feedforward signal which yields to a controller bandwidth of 4 kHz and to a phase margin of 60°. The output voltage control is performed using a PI-type controller with a bandwidth of 20 Hz.

A. Calculated and Measured Efficiency

The losses and efficiency of the implemented rectifier are calculated for $f_N = 400$ Hz using the analytical expressions derived in Section V based on the datasheet specifications (components listed in Table VI). The results of this calculation are given in Table VII.

The losses of the Δ-switch rectifier are dominated by the losses of the semiconductors. The calculated efficiency for the desired input voltage range varies between 94% and 95.2%, and the results are in good agreement with the measurement results given in Fig. 11(a). The measured efficiencies are somewhat lower than the calculated values and the difference has been found in the current-dependent losses of the EMI-filter. These losses have been considered as a constant term in the calculation for the sake of brevity. A three-phase power source [33] is used for testing the rectifier and the output current capability of this power source (5 kW, 13 A_{rms}) limits the power level for the given efficiency measurements. A more sophisticated analysis of the magnetic components showed that the power losses of the magnetic material and losses due to skin and proximity effects can be reduced by an optimized design of the boost inductor and the EMI-filter inductors. The efficiency could approximately be increased by 1% if more suited magnetic devices, e.g., ferrite cores instead of powder cores, are applied.

TABLE VII
CALCULATED POWER LOSS BREAK-DOWN AND EFFICIENCY OF THE PROPOSED Δ-SWITCH RECTIFIER FOR AN OUTPUT POWER OF $P_o = 4$ kW

Input voltage (line rms)	97.7	115	132	V
Input voltage (line-to-line rms)	169	199	229	V
Input current (rms)	14.4	12.2	10.6	A
Modulation index	0.6	0.7	0.81	
Losses				
Switch losses	67.4	54.3	45.3	W
Diode losses	23.9	23.2	22.6	W
Thyristor losses	10.8	10.6	10.3	W
Total semiconductor losses	102.1	88.1	78.2	W
Input choke	34	30	27	W
Output capacitors	12	8	5	W
Auxiliary power	30	30	30	W
Additional losses (EMI,...)	70	70	70	W
Total power losses	249.1	226.1	210.2	W
Efficiency	94.0	94.6	95.1	%

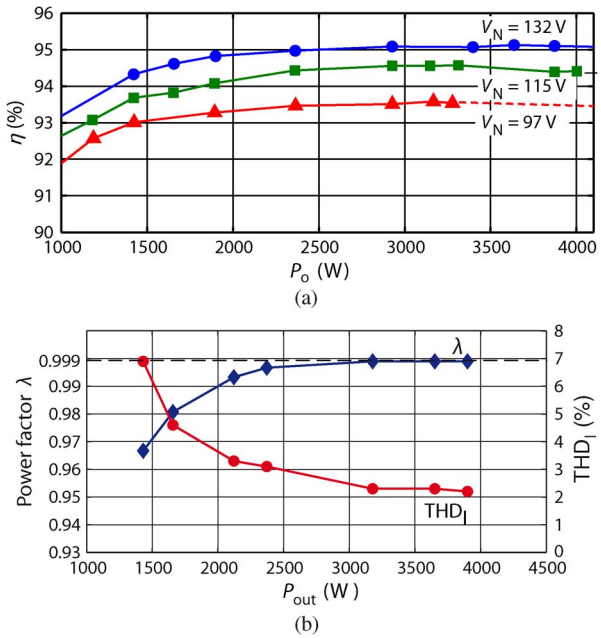

Fig. 11. (a) Measured efficiency of the 5-kW laboratory prototype at $f_N = 400$ Hz for the specified mains voltages and (b) measured power factor λ and input current quality THDI as a function of P_o ($f_N = 400$ Hz and $V_N = 115$ V). The measurements are performed using the three-phase power analyzer DEWE-2600 from Dewetron, Inc.

The measured power factor λ is plotted in Fig. 11(b) together with the measured input current quality (expressed by the THD-value). The power factor and input current quality are measured with the three-phase power analyzer DEWE-2600 from Dewetron Inc. At high power levels a power factor of $\lambda = 0.999$ can be achieved whereas the power factor drops down at partial load. The reason for that can be found in the capacitive current drawn by EMI-filter capacitors. As already mentioned, an existing EMI-filter originally designed for a 50-Hz VR system is applied to the Δ-switch rectifier system. The total amount of input capacitance for a system operated with 360 Hz–800 Hz may be reduced but one has to keep in mind that a specific amount of input capacitance is needed for proper operation of

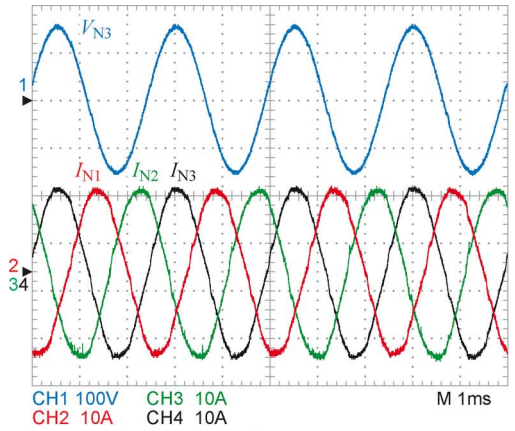

(a)

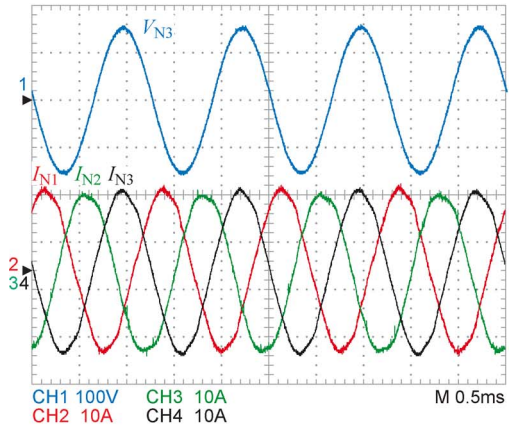

(b)

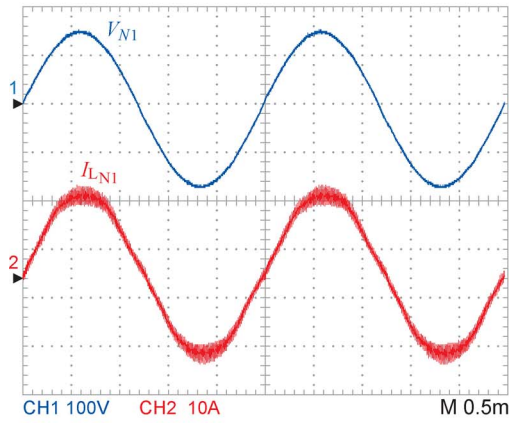

(c)

Fig. 12. Measurement results taken from the laboratory prototype at an output power level of $P_o = 4$ kW using the oscilloscope LeCroy Waverunner LT264M in combination with the Tektronix current clamp A6302; (a) Input currents and phase voltage at $f_N = 400$ Hz ($THD_I = 2.3\%$, $\lambda = 0.999$), (b) at $f_N = 800$ Hz ($THD_I = 2.9\%$, $\lambda = 0.999$), and (c) inductor current $I_{L_{N1}}$ at $f_N = 400$ Hz.

the rectifier system. As analyzed in [36], the Δ-switch rectifier system would be able to compensate a specific amount of phase lag but this is not implemented in the laboratory prototype.

Fig. 11(b) also confirms that a very good input current quality ($THD_I < 4\%$) can be achieved.

B. Experimental Results

The measured input currents of the rectifier are given in Fig. 12(a) for $P_o = 4$ kW, $f_N = 400$ Hz where a THD_I of 2.3% and a power factor of $\lambda = 0.999$ have been measured and Fig. 12(b) shows a measurement of the input currents at $P_o = 4$ kW and $f_N = 800$ Hz. There a THD_I of 2.9% and a power factor of $\lambda = 0.999$ have been measured. In Fig. 12(c) the inductor current $I_{L_{N1}}$ is shown. The current ripple shows its maximum at $\varphi_N = 0°$, is in good agreement with the simulation results, and thus confirms the operation of the proposed current controller.

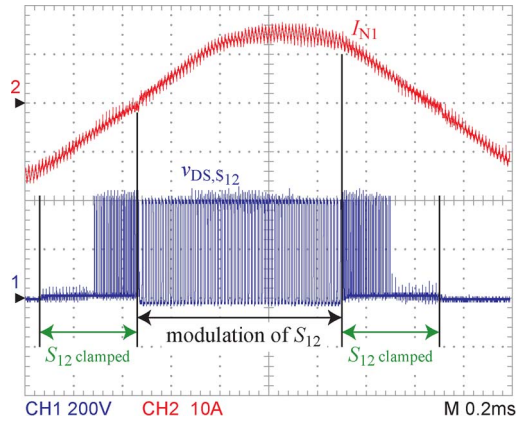

Fig. 13. Measured drain-source voltage v_{DS} of switch S_{12} at an output power level of $P_o = 4$ kW.

As mentioned in Section V, the commutation paths include four semiconductor devices. It is therefore difficult to minimize the parasitic inductance of this path in practice. The result is a considerable ringing of the MOSFETs drain-source voltages. In Fig. 13, a measurement of the drain-source voltage v_{DS} of switch S_{12} is shown. Although the layout has been optimized to minimize the commutation path inductance, a voltage overshoot of $\approx$60 V can be observed if the switch is PWM-operated. In addition the MOSFET, as depicted in Fig. 13, experiences a PWM-shaped blocking voltage, originating from the two other switches while the device is clamped into permanently off-state (S_{12} in $\varphi_N \in [30°, \ldots, 90°, 210°, \ldots, 270°]$). This voltage overshoot is unfortunately even higher than the over-voltage generated from the switch itself which has to be considered in the system design.

Fig. 14 shows the measured behavior of the rectifier system on a single phase loss at $P_o = 2.25$ kW and $f_N = 400$ Hz. As illustrated in Fig. 14(a) phase L_1 is therefore disconnected from the power source. In consonance to the simulation results given in Fig. 8 the system further operates in two phase mode without any changes in the controller structure [cf., Fig. 14(b)]. During two phase operation, a pulsed power flow from the mains to the rectifier output with a frequency of $2f_N$ occurs which results in a output voltage ripple. Note that this voltage ripple cannot be seen in the measurement given in Fig. 14(b) due to the large output capacitance (1.47 mF) and the unfavorable scaling of the output voltage.

In a practical implementation, an EMI-filter with DM-capacitors (C_{DMi}) after the boost inductors is connected to the input of the rectifier system. Together with the boost inductors, these filter capacitors form a resonant tank which is excited by the switching actions of the corresponding switches S_{ij}. If phase L_1 is disconnected from the mains the input currents on the two remaining phases (L_2 and L_3) are controlled by

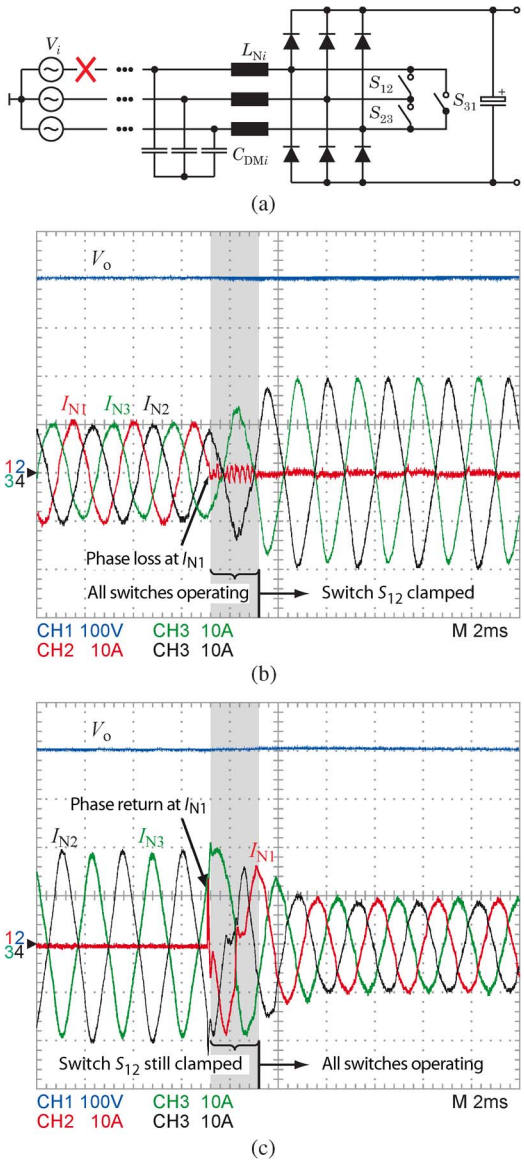

Fig. 14. Measured response of the rectifier system on a single phase loss at phase L_1 ($P_o = 2.25$ kW and $f_N = 400$ Hz); (a) Simplified schematic including first EMI-filter stage, (b) measured inductor currents I_{Ni} and output voltage V_o at phase loss, and (c) return of the phase voltage.

the switching actions of switch S_{23}. In addition, more or less random switching actions on the two remaining switches occur if the controller structure is not changed. If both switches are turned on (S_{12} and S_{31}), the switch S_{23} is shortened by these two switches and the (random) switching actions also influence the input currents on the two remaining phases. As a result, in contrast to the simulation results given in Fig. 8, a relative pronounced current oscillation in the boost inductor of the disconnected phase occurs [cf., gray shaded area in Fig. 14(b)]. A simple RC-snubber circuit could be connected in parallel to the DM-capacitors in order to damp this unwanted oscillations but the power dissipation of the snubber resistor would be far to high for a mains frequency of $f_N = 800$ Hz. A much better solution is to clamp one of the two switches (e.g., S_{12}) during two-phase operation which is finally implemented in the rectifier system. Thereto, a possible phase loss has to be detected which can for instance be done by the rms-measurement of the input voltages (which is typically needed for output voltage control). In Fig. 14(b) the phase loss is approximately detected after half a period and switch S_{12} is clamped to permanently off-state. After this additional clamping action, no oscillations occur.

Fig. 14(c) shows the behavior of the rectifier system if phase L_1 is up again. Due to the clamping action of S_{12}, the rectifier system is not able to generate sinusoidal input currents [cf., gray shaded area in Fig. 14(c)] but the amplitude of the currents is still limited. After approximately half a period, the control system detects that the corresponding phase is up again and the clamped switch S_{12} is released. This confirms that the rectifier system is able to handle a single phase loss at a reduced power level. In theory, a change of the controller structure is not necessary but in practice appearing current oscillations can be prevented if one of the remaining switches is clamped to permanently off-state.

In order to get a basic idea of the conducted emissions of the Δ-switch rectifier, initial EMI-measurements of the rectifier were performed at an input frequency of $f_N = 50$ Hz. A standard LISN according to CISPR 16 (50 μH, 50 Ω) [34] was used for that purpose. A three-phase DM/CM noise separator [37] was applied to measure the DM and CM noise separately. The measurements were done without a specific EMI-filter, but to provide proper operation of the rectifier capacitors of 3.4 μF per phase have been placed at the input of the rectifier in star connection. In the airborne standard DO160D [35] emission limits for the noise currents are defined, but only noise voltage measurements have been performed. Taking the frequency-dependent impedance of the LISN into consideration, the required current noise levels have been calculated using the measured noise voltages. More information about this calculation can be found in [38]. The results of the peak-measurements and subsequent calculations for the frequency range 150 kHz...30 MHz are shown in Fig. 15 together with the limits of the airborne standard DO160D (Category B and Category L, M, H). According to Fig. 15, CM emissions dominate the emissions of the converter. Accurate modeling of the parasitic CM-paths and careful design of the CM filter stage are essential. The total amount of input capacitors ($C_{DM} = 3.4$ μF) would almost be sufficient for DM noise and this type of emissions can therefore be handled by a multistage LC-filter.

VII. Comparison With Vienna Rectifier

In order to be able to benchmark the characteristics of the proposed Δ-switch rectifier a 6-switch Vienna-type rectifier [cf. Fig. 1(a)] is used as a reference. Both rectifiers are designed to obtain the specifications listed in Table V. The same semiconductors and power components as listed in Table VI and also a nearly identical mechanical construction are used for the VR system. According to Table VIII, three more diodes are required for the VR, but these diodes are only commutated with the supplying mains frequency and are therefore relatively inexpensive. The D_{N-} diodes of the Vienna-type rectifier are replaced by the start-up thyristors; no additional elements are thus needed for start-up. The Δ-switch rectifier shows a slightly

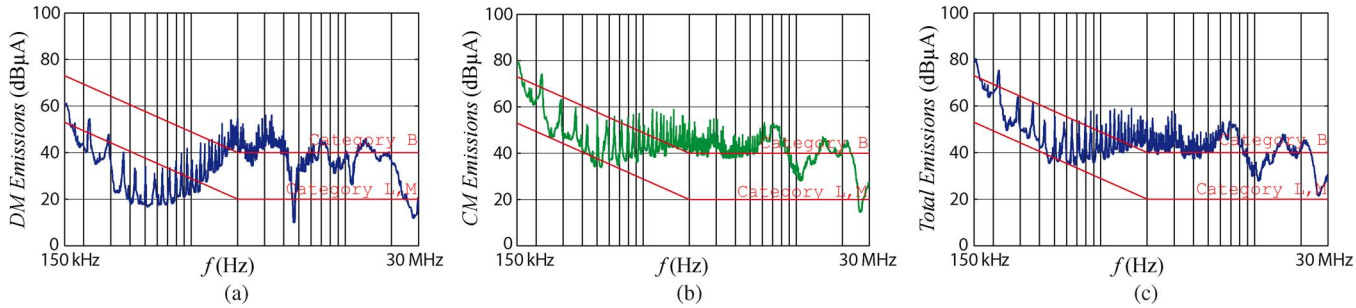

Fig. 15. First CE measurements using the EMI test receiver ESPI3 from Rhode & Schwarz; (a) DM emissions, (b) CM emissions, and (c) total conducted emissions without EMI-Filter.

TABLE VIII
COMPARISON OF THE PROPOSED Δ-SWITCH RECTIFIER WITH A 6-SWITCH VIENNA-TYPE RECTIFIER

	Δ-switch rectifier	**6-switch Vienna-type rectifier**
Num. of switches	6	6
Num. of diodes	6	9
Num. of thyristors	3	3
Output voltage	400 V	400 V
Output power	5 kW	5 kW
Efficiency (@115V/5kW)	94.9%	94.4%
Power density	$1.91\,\mathrm{kW/dm^3}$	$1.91\,\mathrm{kW/dm^3}$
Power weight ratio	1.32 kW/kg	1.32 kW/kg

better efficiency compared to the Vienna-type rectifier system at equal size and power density. The same magnetic materials as used for the Δ-switch rectifier have been used and, as discussed in Section VI-A, the total efficiency can also be increased by approximately 1% for the Vienna-type rectifier if an enhanced magnetic material is used. If the output voltage of the Vienna-type rectifier is increased to $V_\mathrm{o} = 800$ V, the Vienna-type rectifier is able to handle input voltages up to $V_\mathrm{N,ll} = 440\ V_\mathrm{rms}$ and an output power of $P_\mathrm{o} = 10$ kW which increases its power density considerably. The Δ-switch rectifier is the optimal choice for the desired mains voltage of 115 V_rms and a corresponding output voltage of $V_\mathrm{o} = 400\ V_\mathrm{dc}$.

VIII. CONCLUSION

This paper presents the design of a unidirectional 5-kW three-phase Δ-switch rectifier focused to the application in aircraft systems with a mains voltage of 115 V_rms. The Δ-switch rectifier is a very interesting choice for the desired mains voltage level as MOSFET devices can be applied. In addition, the rectifier system shows small conduction losses due to the Δ-connected switches. The proposed control concept allows to directly control the phase currents and even a single phase loss can be handled by the controller concept without changing the controller structure. The discussed implementation of the pulse-width modulator, where the phase-related modulation signals have to be mapped to the Δ-connected switches using a star-delta transformation, results in switching sequences with minimum switching actions and minimum conduction losses. Analytical expressions for the component stresses that simplify the design and dimensioning of the system are derived. A $\mathrm{THD_I}$ of 2.3% at $f_\mathrm{N} = 400$ Hz and an efficiency of 94.6% at $P_\mathrm{o} = 4$ kW have been achieved with the prototype as built, which results in a power density of 1.91 kW/dm^3 and a power to weight ratio of 1.32 kW/kg. The quite limited efficiency could be increased by approximately 1% if a more sophisticated design of the EMI-filter and the magnetic components was made. The reduction of core losses can be achieved if ferrite cores are used instead of the unsuited powder cores. Measurements taken from the-5 kW laboratory prototype confirm the high performance of the proposed current controller using the derived PWM-modulation scheme. A comparison of the Δ-switch rectifier with a 6-switch Vienna-type rectifier confirms a slightly higher efficiency for the Δ-switch rectifier for the desired mains voltage range. Due to the reduced semiconductor voltage stress of the 6-switch Vienna-type rectifier topology, the Vienna-type rectifier system would, however, be an ideal candidate for the increased mains voltage of 230 V_rms of future aircraft.

REFERENCES

[1] D. R. Trainer and C. R. Whitley, "Electric actuation—Power quality management of aerospace flight control systems," in *Proc. Int. Conf. Power Electron., Mach. Drives*, Jun. 4–7, 2002, pp. 229–234.
[2] J. A. Rosero, J. A. Ortega, E. Aldabas, and L. Romeral, "Moving towards a more electric aircraft," *IEEE Aerosp. Electron. Syst. Mag.*, vol. 22, no. 3, pp. 3–9, Mar. 2007.
[3] C. R. Avery, S. G. Burrow, and P. H. Mellor, "Electrical generation and distribution for the more electric aircraft," in *Proc. 42nd Int. UPEC*, Sep. 4–6, 2007, pp. 1007–1012.
[4] E. Lavopa, P. Zanchetta, M. Sumner, and F. Cupertino, "Real-time estimation of fundamental frequency and harmonics for active shunt power filters in aircraft electrical systems," *IEEE Trans. Ind. Electron.*, vol. 56, no. 8, pp. 2875–2884, Aug. 2009.
[5] H. Zhang, F. Mollet, C. Saudemont, and B. Robyns, "Experimental validation of energy storage system management strategies for a local dc distribution system of More Electric Aircraft," *IEEE Trans. Ind. Electron.*, vol. 57, no. 12, p. 3905, Feb. 25, 2010.
[6] A. S. Lopez, P. Zanchetta, P. W. Wheeler, A. Trentin, and L. Empringham, "Control and implementation of a matrix-converter-based ac ground power-supply unit for aircraft servicing," *IEEE Trans. Ind. Electron.*, vol. 57, no. 6, pp. 2076–2084, Jun. 2010.
[7] R. Lai, F. Wang, R. Burgos, Y. Pei, D. Boroyevich, B. Wang, T. A. Lipo, V. D. Immanuel, and K. J. Karimi, "A systematic topology evaluation methodology for high-density three-phase PWM ac–ac converters," *IEEE Trans. Power Electron.*, vol. 23, no. 6, pp. 2665–2680, Nov. 2008.
[8] G. Gong, M. L. Heldwein, U. Drofenik, J. Minibock, K. Mino, and J. W. Kolar, "Comparative evaluation of three-phase high-power-factor ac–dc converter concepts for application in future more electric aircraft," *IEEE Trans. Ind. Electron.*, vol. 52, no. 3, pp. 727–737l, Jun. 2005.

[9] Y. Zhao, Y. Li, and T. A. Lipo, "Force commutated three level boost type rectifier," *IEEE Trans. Ind. Appl.*, vol. 31, no. 1, pp. 155–161, Jan./Feb. 1995.
[10] J. Minibock and J. W. Kolar, "Novel concept for mains voltage proportional input current shaping of a VIENNA rectifier eliminating controller multipliers," *IEEE Trans. Ind. Electron.*, vol. 52, no. 1, pp. 162–170, Feb. 2005.
[11] J. C. Salmon, "Comparative evaluation of circuit topologies for 1-phase and 3-phase boost rectifiers operated with a low current distortion," in *Proc. Canadian Conf. Elect. Comput. Eng.*, Sep. 25–28, 1994, vol. 1, pp. 30–33.
[12] J. C. Salmon, "Reliable 3-phase PWM boost rectifiers employing a stacked dual boost converter subtopology," *IEEE Trans. Ind. Appl.*, vol. 32, no. 3, pp. 542–551, May/Jun. 1996.
[13] J. C. Salmon, "3-phase PWM boost rectifier circuit topologies using 2-level and 3-level asymmetrical half-bridges," in *Proc. 10th Annu. APEC*, Mar. 5–9, 1995, vol. 2, pp. 842–848.
[14] N. Mohan, "A novel approach to minimize line-current harmonics in interfacing power electronics equipment with 3-phase utility systems," *IEEE Trans. Power Del.*, vol. 8, no. 3, pp. 1395–1401, Jul. 1993.
[15] R. Naik, M. Rastogi, and N. Mohan, "Third-harmonic modulated power electronics interface with three-phase utility to provide a regulated DC output and to minimize line-current harmonics," *IEEE Trans. Ind. Appl.*, vol. 31, no. 3, pp. 598–602, May/Jun. 1995.
[16] H. Yoo and S. Sul, "A novel approach to reduce line harmonic current for a three-phase diode rectifier-fed electrolytic capacitor-less inverter," in *Proc. 24th Annu. IEEE APEC*, Feb. 15–19, 2009, pp. 1897–1903.
[17] J. C. Salmon, "Operating a three-phase diode rectifier with a low-input current distortion using a series-connected dual boost converter," *IEEE Trans. Power Electron.*, vol. 11, no. 4, pp. 592–603, Jul. 1996.
[18] J. W. Kolar, H. Ertl, and F. C. Zach, "Realization considerations for unidirectional three-phase PWM rectifier systems with low effects on the mains," in *Proc. 6th Int. Conf. PEMC*, Budapest, Hungary.
[19] R.-J. Tu and C.-L. Chen, "A new three-phase space-vector-modulated power factor corrector," in *Proc. 9th Annu. IEEE APEC*, Feb. 13–17, 1994, vol. 2, pp. 725–730.
[20] P. Bialoskorski and W. Koczara, "Unity power factor three phase rectifiers," in *Proc. 24th Annu. IEEE Power Electron. Spec. Conf.*, Jun. 20–24, 1993, pp. 669–674.
[21] W. Koczara and P. Bialoskorski, "Controllability of the simple three phase rectifier operating with unity power factor," in *Proc. 5th Eur. Conf. Power Electron. Appl.*, Sep. 13–16, 1993, vol. 7, pp. 183–187.
[22] D. Carlton, W. G. Dunford, and M. Edmunds, "Continuous conduction mode operation of a three-phase power factor correction circuit with quasi tri-directional switches," in *Proc. 30th Annual IEEE Power Electron. Spec. Conf.*, Aug. 1999, vol. 1, pp. 205–210.
[23] D. Carlton, W. G. Dunford, and M. Edmunds, "Deltafly' three-phase boost power factor correction circuit operating in discontinuous conduction mode," in *Proc. IEEE Int. Symp. ISIE*, 1999, vol. 2, pp. 533–538.
[24] D. Carlton, W. G. Dunford, and M. Edmunds, "SEPIC 3-phase 3-switches power factor correction circuit operating in discontinuous conduction mode," in *Proc. IEEE ISIE*, Jul. 7–10, 1998, vol. 1, pp. 81–86.
[25] M. P. Kazmierkowski and L. Malesani, "Current control techniques for three-phase voltage-source PWM converters: A survey," *IEEE Trans. Ind. Electron.*, vol. 45, no. 5, pp. 691–703, Oct. 1998.
[26] A. Limas, C. Cruz, and F. Antunes, "A new low cost AC-DC converter with high input power factor," in *Proc. 22nd IEEE IECON*, Aug. 5–10, 1996, vol. 3, pp. 1808–1813.
[27] R. J. Tu and C. L. Chen, "A new space-vector-modulated control for a unidirectional three-phase switch-mode rectifier," *IEEE Trans. Ind. Electron.*, vol. 45, no. 2, pp. 256–262, Apr. 1998.
[28] C. Qiao and K. M. Smedley, "A general three-phase PFC controller for rectifiers with a parallel-connected dual boost topology," *IEEE Trans. Power Electron.*, vol. 17, no. 6, pp. 925–934, Nov. 2002.
[29] N. Noor, J. Ewanchuk, and J. C. Salmon, "PWM current controllers for a family of 3-switch utility rectifier topologies," in *Proc. CCECE*, Apr. 22–26, 2007, pp. 1141–1144.
[30] M. Hartmann, J. Miniboeck, and J. W. Kolar, "A three-phase delta switch rectifier for more electric aircraft applications employing a novel PWM current control concept," in *Proc. 24th Annu. IEEE APEC*, Feb. 15–19, 2009, pp. 1633–1640.
[31] M. Hartmann, H. Ertl, and J. W. Kolar, "EMI filter design for a 1 MHz, 10 kW three-phase/level PWM rectifier," *IEEE Trans. Power Electron.*, 2010.
[32] M. Chen and J. Sun, "Feedforward current control of boost single-phase PFC converters," *IEEE Trans. Power Electron.*, vol. 21, no. 2, pp. 338–345, Mar. 2006.
[33] *SmartWave Switching Amplifier SW5250A, Operation Manual*, Elgar Electronics Corp., 2008. [Online]. Available: http://www.elgar.com
[34] IEC Internationl Special Committee on Ratio Interference—C.I.S.P.R., C.I.S.P.R. Specification for Radio Interference Measuring Apparatur and Measurement Methods—Publication 16, Geneve, Switzerland, 1977.
[35] RTCA Inc., Enviromental Conditions and Test Procedures for Airborne Equipment—RTCA DO-160D.
[36] S. K. T. Miller and J. Sun, "Comparative study of three-phase PWM rectifiers for wind energy conversion," in *Proc. 21st APEC*, Mar. 19–23, 2006, pp. 937–943.
[37] M. L. Heldwein, J. Biela, H. Ertl, T. Nussbaumer, and J. W. Kolar, "Novel three-phase CM/DM conducted emission separator," *IEEE Trans. Ind. Electron.*, vol. 56, no. 9, pp. 3693–3703, Sep. 2009.
[38] T. Nussbaumer, M. L. Heldwein, and J. W. Kolar, "Differential mode input filter design for a three-phase buck-type PWM rectifier based on modeling of the EMC test receiver," *IEEE Trans. Ind. Electron.*, vol. 53, no. 5, pp. 1649–1661, Oct. 2006.

Michael Hartmann (S'08) received the B.S. (with honors) and M.Sc. degrees (with honors) in electrical engineering from the University of Technology Vienna, Vienna, Austria, in 2005 and 2006, respectively. He is currently working toward the Ph.D. degree at the Power Electronic Systems Laboratory, ETH Zurich, Zurich, Switzerland.

Currently, he is engaged in research on active three-phase rectifiers with ultrahigh switching frequencies at the Power Electronic Systems Laboratory, Swiss Federal Institute of Technology, Zurich. Earlier, he was engaged in research on switched-mode power amplifiers using multicell topologies.

Johann Miniboeck studied Industrial Electronics at the University of Technology Vienna, Vienna, Austria, and received the Dipl.-Ing. (M.Sc.) and Ph.D. degrees at the Power Electronics System Laboratory, ETH Zurich, Zurich, Switzerland, in 1998 and 2008.

Now he is teaching electrical machines, drives, and power electronics at a technical college and is owner of a company on consultancy in power electronics. He has performed various research projects in the field of single-phase and three-phase power factor correction circuits, switch-mode power supplies for various applications and has developed laboratory setups for teaching power electronics and drives. He is the author/coauthor of 36 scientific papers and patents. The current research activities of him are focused on the implementation of single- and three-phase electric vehicle chargers as well as ultra-efficient power factor correction circuits.

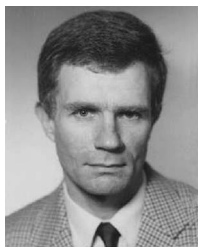

Hans Ertl (M'93) received the Dipl.-Ing. (M.Sc.) and Ph.D. degrees in industrial electronics from the University of Technology Vienna, Vienna, Austria, in 1984 and 1991, respectively.

Since 1984, he has been with the Vienna University of Technology, where he is currently an Associate Professor with the Power Electronics Section of the Institute of Electrical Drives and Machines. He has performed numerous industrial and scientific research projects in the areas of field-oriented control of ac drive systems, switch-mode power supplies for welding and industrial plasma processes, and active rectifier systems. He is the author or coauthor of numerous scientific papers and patents. His current research activities are focused on switch-mode power amplifiers and multicell topologies, in particular, for the generation of testing signals, for active ripple current compensators, and for several applications in the area of renewable energy systems.

Johann W. Kolar (F'10) received the M.Sc. and Ph.D. degrees (*summa cum laude*/promotio sub auspiciis praesidentis rei publicae) from the University of Technology Vienna, Vienna, Austria.

Since 1984, he has been working as an independent international consultant in close collaboration with the University of Technology Vienna, in the fields of power electronics, industrial electronics, and high-performance drives. He has proposed numerous novel PWM converter topologies, and modulation and control concepts, e.g., the VIENNA Rectifier and the Three-Phase ac-ac Sparse Matrix Converter. He has published over 350 scientific papers in international journals and conference proceedings and has filed 75 patents. He was appointed Professor and Head of the Power Electronic Systems Laboratory at the Swiss Federal Institute of Technology (ETH), Zurich, on Feb. 1, 2001. The focus of his current research is on ac-ac and ac-dc converter topologies with low effects on the mains, e.g., for power supply of data centers, More-Electric-Aircraft and distributed renewable energy systems. Further main areas of research are the realization of ultra-compact and ultra-efficient converter modules employing latest power semiconductor technology (e.g., SiC), novel concepts for cooling and EMI filtering, multi-domain/scale modeling/simulation and multi-objective optimization, physical model-based lifetime prediction, pulsed power, and ultra-high speed and bearingless motors.

Dr. Kolar received the Best Transactions Paper Award of the IEEE Industrial Electronics Society in 2005, the Best Paper Award of the ICPE in 2007, the 1st Prize Paper Award of the IEEE IAS IPCC in 2008, the IEEE IECON Best Paper Award of the IES PETC in 2009, the 2009 IEEE Power Electronics Society Transaction Prize Paper Award and the 2010 Best Paper Award of the IEEE/ASME TRANSACTIONS ON MECHATRONICS. He also received an Erskine Fellowship from the University of Canterbury, New Zealand, in 2003. He initiated and/or is the founder/co-founder of 4 spin-off companies targeting ultra-high speed drives, multi-domain/level simulation, ultra-compact/efficient converter systems, and pulsed power/electronic energy processing. In 2006, the European Power Supplies Manufacturers Association (EPSMA) awarded the Power Electronics Systems Laboratory of ETH Zurich as the leading academic research institution in Power Electronics in Europe. He is a Fellow of the IEEE and a Member of the IEEJ and of International Steering Committees and Technical Program Committees of numerous international conferences in the field (e.g., Director of the Power Quality Branch of the International Conference on Power Conversion and Intelligent Motion). He is the founding Chairman of the IEEE PELS Austria and Switzerland Chapter and Chairman of the Education Chapter of the EPE Association. From 1997 through 2000 he has been serving as an Associate Editor of the IEEE TRANSACTIONS ON INDUSTRIAL ELECTRONICS and since 2001 as an Associate Editor of the IEEE TRANSACTIONS ON POWER ELECTRONICS. Since 2002 he also is an Associate Editor of the Journal of Power Electronics of the Korean Institute of Power Electronics and a member of the Editorial Advisory Board of the IEEJ Transactions on Electrical and Electronic Engineering.